Polygonal Eyewall Asymmetries During the Rapid Intensification of Hurricane Michael (2018)

Ting-Yu Cha[1] (ID), Michael M. Bell[1] (ID), Wen-Chau Lee[2], and Alexander J. DesRosiers[1] (ID)

[1]Department of Atmospheric Science, Colorado State University, Fort Collins, CO, USA, [2]National Center for Atmospheric Research, Boulder, CO, USA

Abstract Polygonal eyewall asymmetries of Hurricane Michael (2018) during rapid intensification (RI) are analyzed from ground-based single Doppler radar. Here, we present the first observational evidence of the evolving wind field of a polygonal eyewall during RI to Category 5 intensity by deducing the axisymmetric and asymmetric winds at 5-min intervals. Spectral time decomposition of the retrieved tangential wind structure shows quantitative evidence of low (1–4) azimuthal wavenumbers with propagation speeds that are consistent with linear wave theory on a radial vorticity gradient, suggesting the presence of rapidly evolving vortex Rossby waves. Dual-Doppler winds from the NOAA P-3 Hurricane Hunter airborne radar provide further evidence of the three-dimensional vortex structure that supports growth of asymmetries during RI. Both reflectivity and tangential wind fields show polygonal structure and propagate at similar speeds, suggesting a close coupling of the dynamics and the convective organization during the intensification.

Plain Language Summary Understanding tropical cyclone (TC) structure and evolution are crucial for improving weather forecasts. Hurricane Michael (2018) was observed by radar imagery to have an evolving polygonal eyewall with elliptical, triangular, and square shapes during rapid intensification (RI). While polygonal eyewall shapes have been seen in previous hurricanes, the corresponding evolution of wind asymmetries has never been quantitatively deduced due to limitations from previous observations. Here, we present the first observational evidence of the evolving wind field of a polygonal eyewall during RI to Category 5 intensity by deducing the winds at 5-min intervals from single-Doppler Next Generation Weather Radar (NEXRAD) observations. The results highlight the value of coastal radar observations to investigate physical mechanisms of TC intensity and structure evolution and will help to improve intensity forecasts in the future.

1. Introduction

Tropical cyclone (TC) internal dynamics are a primary factor impacting the storm evolution in an environment that is favorable for rapid intensification (RI) (Hendricks et al., 2010). Inner core processes are intrinsically less predictable and more difficult to observe in detail than the larger scale environment, which makes forecasts of intensity change particularly challenging. The U.S. coastal Next Generation Weather Radar (NEXRAD) network provides continuous surveillance capability of TCs with high temporal and spatial resolution and can collect valuable data on TC evolution. The axisymmetric and asymmetric tangential winds are able to be retrieved using the Generalized Velocity Track Display (GVTD) technique with single ground-based Doppler radar data (Cha, 2018; Jou et al., 2008), providing insights on the TC dynamics and evolution (Cha, 2018; W.-C. Lee & Bell, 2007; Shimada et al., 2018). Hurricane Michael (2018) was the first Category 5 hurricane to make landfall in the United States since Hurricane Andrew (1992) and caused extensive damage in Florida and Georgia (Beven et al., 2019). Satellite and radar imagery showed evidence of an evolving polygonal eyewall as Michael underwent RI during its approach to Florida. In this study, single-Doppler radar winds from a coastal radar and airborne dual-Doppler wind synthesis are analyzed to provide the first observational evidence of the kinematic structure of a polygonal eyewall during RI to Category 5 intensity.

Polygonal eyewalls are hypothesized to be the result of asymmetric vorticity dynamics that can modulate TC structure and intensity through counter-propagating vortex Rossby waves (VRWs) (Hendricks et al., 2012; Kuo et al., 1999, 2016; Muramatsu, 1986; Schubert et al., 1999). A sign reversal of the mean radial

vorticity gradient that acts as a waveguide for VRWs satisfies the Rayleigh condition for barotropic-baroclinic instability (Montgomery & Shapiro, 1995), which can lead to a breakdown of the potential vorticity (PV) ring and redistribution of eyewall PV and angular momentum (Bell & Montgomery, 2008; Schubert et al., 1999) that can accelerate the mean wind inside the radius of maximum wind (RMW), and promote the contraction of the RMW. The presence of a "ring" of mean vorticity that satisfies the Rayleigh condition can exist in both intensifying and weakening storms depending on intensity (Martinez et al., 2017), suggesting that the vortex dynamics can be complex and VRWs may lead to intensification (Menelaou & Yau, 2014), rapid weakening (Martinez et al., 2019), or steady-state periods (Kossin & Eastin, 2001). J.-D. Lee and Wu (2018) hypothesized that polygonal eyewalls acted as a possible RI mechanism in Typhoon Megi (2010) by enhancing the generation of convective bursts inside the RMW, which then affects the development of the warm-core in the upper tropopause and the vertical alignment of the eyewall. They concluded that maintaining a certain pattern of polygonal eyewall structures within the high inertial stability region for an extended period of time is beneficial to RI.
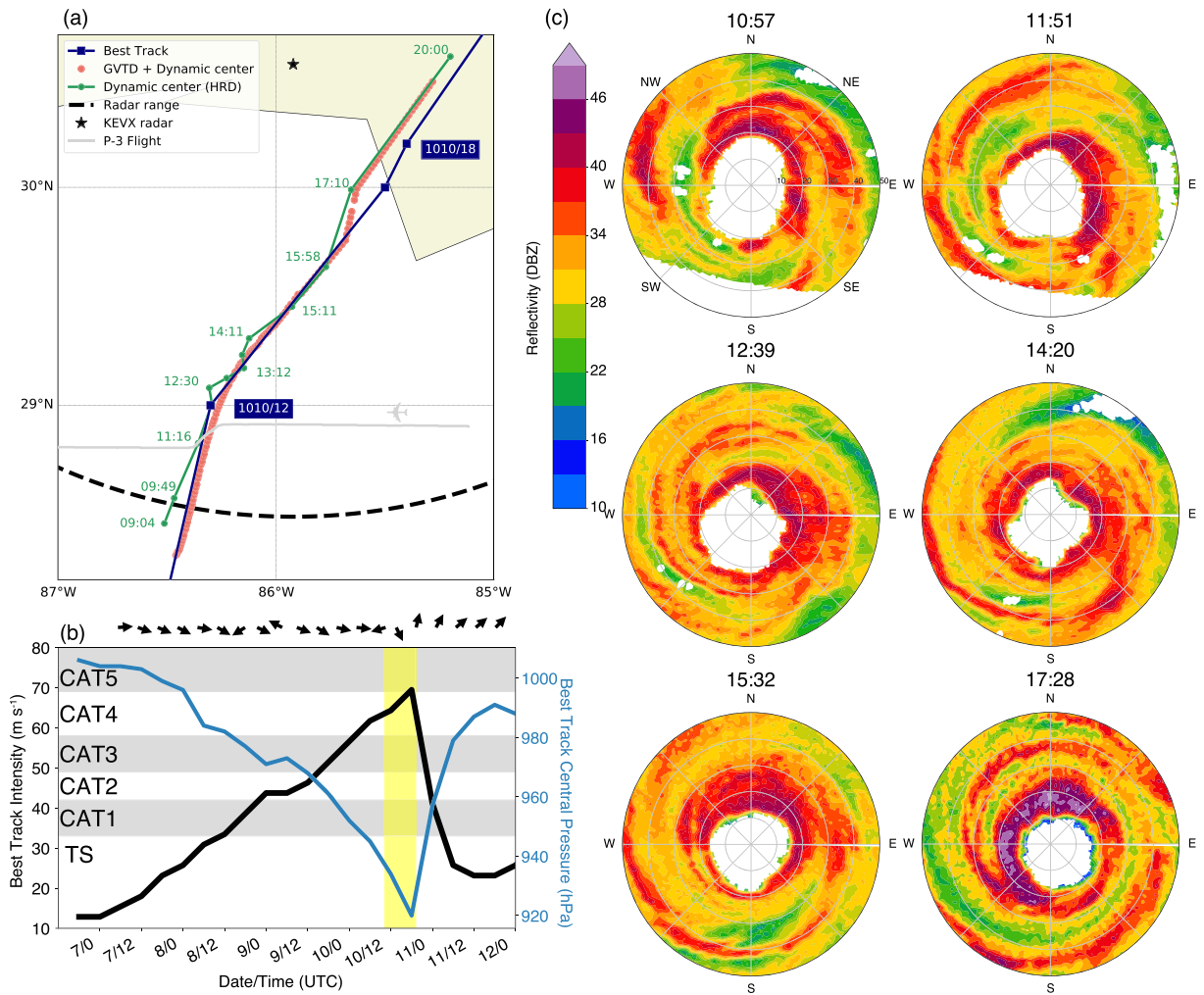
Previous theoretical studies have often used a simplified barotropic nondivergent model framework to investigate the dynamical processes of polygonal eyewalls (Kuo et al., 1999, 2016; Rozoff et al., 2009; Schubert et al., 1999). While this framework can provide substantial insight, it has limitations in investigating eyewall dynamics as moist convective processes are very important to PV generation and the intensification process. Diabatic heating can be introduced as a proxy via a mass sink in shallow-water models (Hendricks et al., 2012, 2014) or simulated directly in 3-D full physics models (Wu et al., 2016), but simulations may not represent the real-world physical mechanisms correctly. Utilizing observational data sets is critical to validate theory and numerical simulations and improve our understanding of polygonal eyewalls in TCs and the relation to intensity change. Prior studies have been limited in their ability to examine the dynamics of VRWs and polygonal eyewalls. Multi-Doppler airborne radar analyses (Reasor et al., 2000) can retrieve the full wind field but have temporal sampling and aliasing limitations (Cha & Bell, 2020; Cha, 2018). Studies analyzing the shape of the eye in reflectivity (Itano & Hosoya, 2013) or using reflectivity as a proxy for PV (Corbosiero et al., 2006) have limitations due to the fact that the reflectivity may not be fully coupled with the winds or PV (Moon & Nolan, 2015).

Analyses of Hurricane Michael (2018) presented herein demonstrate the first observation of high-order VRW propagation using tangential wind asymmetries as a proxy for the PV signal. The results show that the propagation speeds of the waves are consistent with linear wave theory on a vortex and help to provide new insight into physical mechanisms contributing to TC RI. Section 2 describes the observing platform, quality control processes for the observations, and analysis methodology. Section 3 describes Michael's evolution of reflectivity and tangential winds retrieved by the GVTD technique and discusses sampling limitations and the physical mechanisms contributing to Michael's inner core variability. Conclusions and future work are presented in section 4.

2. Data and Methods

Hurricane Michael was within range of ground-based radar surveillance during its approach to the Florida panhandle and brought in devastating winds and storm surge to the coastal area near Mexico Beach and Tyndall Air Force Base (AFB). Figure 1 shows the track, intensity, environmental vertical wind shear (VWS) direction, and reflectivity evolution at 3 km. Michael intensified nearly continuously from genesis to landfall and experienced two RI periods during its life cycle. RI is defined as a 24-hr increase in the maximum sustained wind of 15.4 m s^{-1} (30 kt) (Kaplan & DeMaria, 2003). The second RI started on 9 October and ended when the storm reached Category 5 intensity (140 kt) at the time of landfall around 1730 UTC 10 October. After the landfall, Michael underwent a rapid weakening and extratropical transition as the TC moved into North Carolina. The analysis period for this study is from 1000 to 1930 UTC 10 October when the hurricane was within the coastal radar detection range. The deep layer 200- to 850-hPa VWS magnitude was about 5 m s^{-1} with a transition from northwesterly to south-southeasterly during the analysis period.

Figure 1a shows the TC tracks derived from three different methods: best track, GVTD-simplex, and dynamic aircraft location. The best track centers are surface-based estimates from the National Hurricane Center (NHC) that consider satellite, ground-based radars, aircraft, and in situ measurements every 6 hr. The dynamic aircraft centers from the Hurricane Research Division (HRD) are derived from the NOAA

Figure 1. (a) Three tracks of Hurricane Michael on 10 October 2018 derived from best track from NHC (blue), GVTD-simplex objective centers (red), and aircraft dynamic centers (green) from NOAA HRD. The gray line is P-3 flight track from 1100 to 1130 UTC 10 October. (b) NHC best track wind intensity (black) and minimum central pressure (blue). The black arrow on the top row is the vertical wind shear direction (black) from the Statistical Hurricane Intensity Prediction Scheme (SHIPS) database (DeMaria et al., 2005). Yellow bar indicates the analysis period. (c) KEVX radar reflectivity scans at 1057, 1151, 1239, 1420, 1532, and 1728 UTC. The sequence of figures is from left to right and from top to bottom. The interval of concentric circles is 10 km.

P-3 (hereafter as P-3) in situ measurements of wind and geopotential height at 700 hPa (Willoughby & Chelmow, 1982). The GVTD-simplex objective centers are obtained from the radar data at 3-km altitude using a simplex method to obtain a set of possible circulation centers (Lee et al., 1999; Lee & Marks, 2000) that are selected by an objective algorithm (Bell & Lee 2012) to smooth the track and reduce the center uncertainty. The tracks derived from the three different methods have similar trends in the earlier period, while the dynamic centers show a trochoidal motion between 1200 and 1400 UTC. Two hours before landfall, the three tracks started to diverge, likely due to the difference in height of the estimates and the impact of surface friction and VWS. In this study, we use the combination of GVTD objective centers from 1000 to 1530 UTC and dynamic centers from 1530 to 1930 UTC for the analysis because the GVTD-simplex algorithm cannot find the center accurately when the storm is too close to the radar.

Data from the NEXRAD radar in Eglin AFB, Florida (KEVX) were analyzed from 1000 to 1930 UTC 10 October. The radar sweep files were processed with Lidar Radar Open Software Environment (LROSE) software (Bell, 2019) and the National Center for Atmospheric Research (NCAR) SoloII software (Bell et al., 2013) to correct Doppler velocity aliasing and remove the nonmeteorological echoes. The edited sweep files were then gridded using interpolation of the fields from plan position indicators (elevation angle, Y, Z) to

constant-altitude plan position indicators in Cartesian coordinate (X, Y, Z). The gridded data were further analyzed by the Vortex Objective Radar Tracking and Circulation (VORTRAC) software, and the GVTD technique was used to retrieve the kinematic structure (Cha & Bell, 2020; Cha, 2018; Jou et al., 2008). The GVTD algorithm can retrieve the axisymmetric and asymmetric components of tangential winds and axisymmetric radial wind. Since the GVTD algorithm has no approximation to the geometry, the GVTD-derived higher wavenumbers will not be distorted in phase as long as the amplitude of that wavenumber can be detected by a Doppler radar.

In addition to the ground-based radar data, the P-3 aircraft flew a reconnaissance mission from 0800 to 1400 UTC 10 October and collected high-resolution airborne Doppler radar data. The flight pass from 1100 to 1130 UTC 10 October is analyzed in detail for this study to examine the 3-D kinematic structure from dual-Doppler synthesis using the SAMURAI variational analysis technique (Bell, Montgomery, et al., 2012).
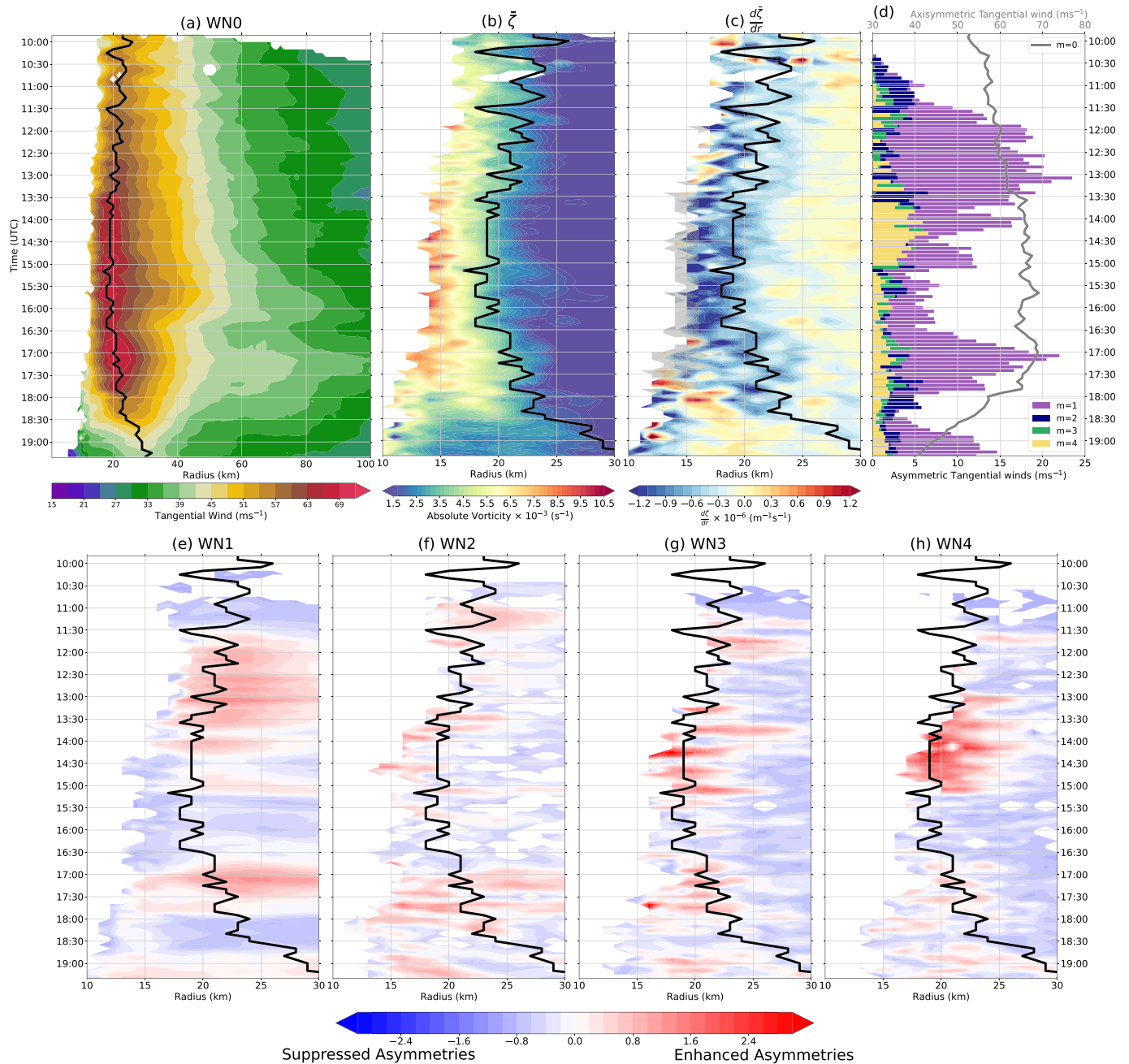
3. Results

Figure 1c shows a sequence of reflectivity images on 10 October that indicate intensification was accompanied by evolving reflectivity asymmetry. Hurricane Michael exhibited many noncircular eyewall shapes including ellipses, triangles, squares, and hexagons, which transitioned from low to high to low wavenumbers and then axisymmetrized. Most of the high-order features were short-lived, with the exception of an elliptical eyewall that was traceable for an hour (1030–1130 UTC) with reflectivity maximized near the ends of the major ellipse axis at 1057 UTC. An hour later, the elliptical eyewall evolved into a triangle shape with reflectivity maximized on the eastern side. The asymmetries continued rotating cyclonically along the eyewall, and the eyewall became an irregular shape associated with spiral bands circulating around the eye at 1239 UTC. Michael's eyewall shape transitioned to a square at 1420 UTC, a quasi-triangle at 1532 UTC, and eventually axisymmetrized to a near round circle. After Michael made landfall at 1730 UTC, the reflectivity decreased in the southeast eyewall, while the northwestern quadrant had some of the highest reflectivity values during the analysis period exceeding 45 dBZ, suggesting an increasing impact of surface friction and shear.

Figure 2 shows a time-radius diagram of retrieved wind and derived dynamical quantities. The wavenumber 0 (axisymmetric) tangential wind (Figure 2a) generally intensified until landfall with a broadening outer wind field out to 100-km radius. The mean tangential wind reached its maximum intensity ($\sim$65 m s^{-1}) around 1700 UTC then decayed due to land interaction and increasing shear throughout the rest of analysis period. Figures 2b and 2c show the evolution of eyewall axisymmetric vorticity and its radial gradient out to 30-km radius. The corresponding amplitude of the wavenumber 0–4 tangential wind components is shown in Figure 2d, with the black line denoting the peak axisymmetric wind and bars denoting the asymmetric components. Due to the difference in magnitude of the asymmetric components, the normalized amplitude is shown in Figures 2e–2h using the time-mean value of each wavenumber within the eyewall region as a normalization factor, such that $V_{\mathrm{norm},\,m} = (V_m - \overline{V_m})/\overline{V_m}$, where V_m is the instantaneous amplitude for each wavenumber m and $\overline{V_m}$ is the time-mean value of the amplitude averaged between RMW − 5 km and RMW + 5 km from 1000 to 1930 UTC. The normalization more clearly visualizes the relative changes in asymmetric tangential wind with warm colors denoting enhanced asymmetries and cool colors denoting reduced asymmetries. The relative changes in asymmetric tangential wind are not very sensitive to the averaging radii.

Early in the analysis period around 1030 UTC, the elliptical eyewall seen in the radar reflectivity (Figure 1c) is also evident in the retrieved wavenumber 2 tangential wind component (Figure 2f). By 1130 UTC, both wavenumber 1 and 3 components strengthened (Figures 2e and 2g). Between 1200 to 1330 UTC, the eyewall was dominated by a wavenumber 1 asymmetry that continued to intensify up to $\sim$23 m s^{-1}. Enhanced wavenumber 1 asymmetry is usually diagnosed as a result from the VWS impact, but the local VWS magnitude from the P-3 flight radar analysis was only 2.9 m s^{-1}, suggesting that VWS was not the cause of the increasing wavenumber 1 asymmetry. The GVTD analysis and P-3 in situ data suggest that wavenumber 1 asymmetries seemed more likely to be connected to internal processes in the inner core due to the presence of a trochoidal oscillation of the center at this time. Around 1300 UTC as the wavenumber 1 was near its maximum amplitude, the higher order asymmetries were suppressed, and the mean vorticity in the inner core decreased
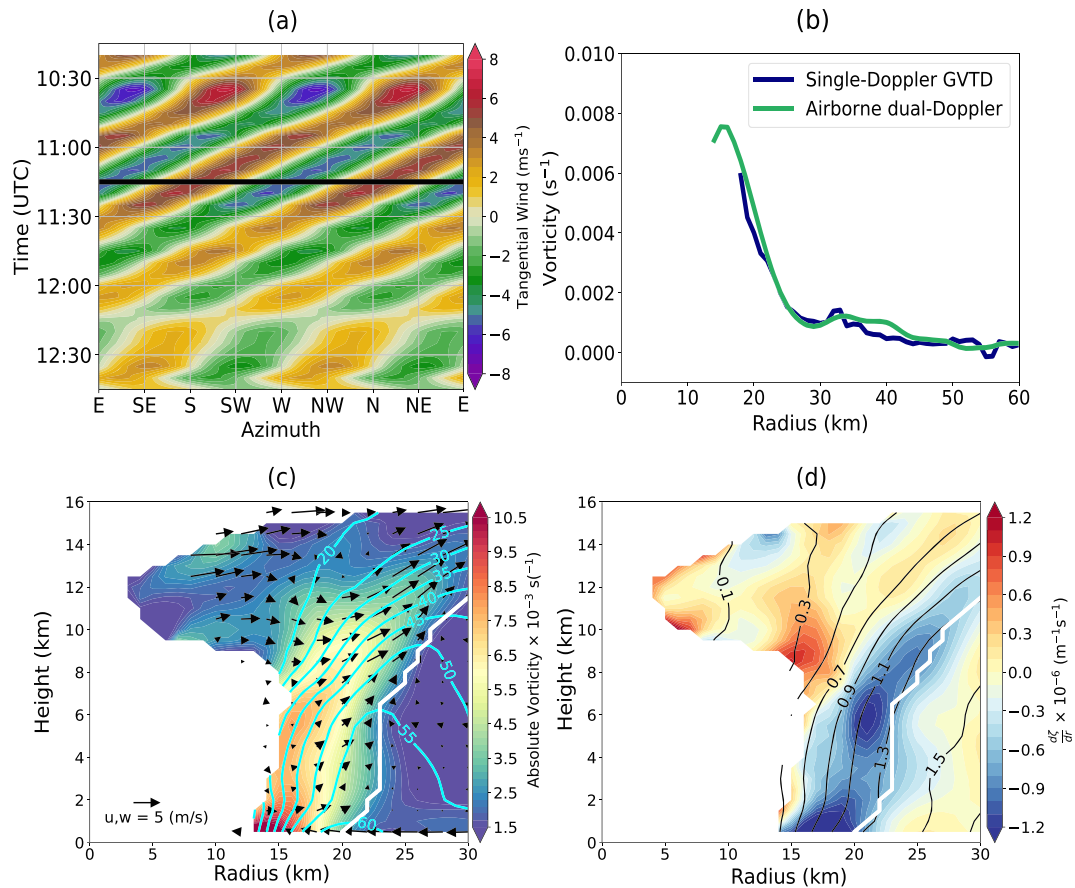
Figure 2. Single-Doppler radar data collected in Hurricane Michael between 1000 and 1930 UTC 10 October 2018. Time-radius diagram of the (a) wavenumber 0 tangential wind, (b) mean vertical vorticity, (c) mean radial vertical vorticity gradient at $z = 3$ km. (d) Time series of maximum amplitude of wavenumbers from $m = 0$–4. Time-radius diagram of the $m = 1$–4 normalized tangential wind at $z = 3$ km for (e)–(h). The black line in (a)–(c) and (e)–(h) indicates the radius of maximum wavenumber 0 tangential wind.

slightly. The analysis shows an appearance of a sign reversal of the mean radial vorticity gradient inside the RMW around 1230 UTC, suggesting the onset of dynamic instability.

One hypothesis for the wavenumber 1 asymmetry evolution as an algebraic instability was proposed by Smith and Rosenbluth (1990) and Nolan and Montgomery (2000). The algebraic instability is different from the barotropic instability, and the initial condition requires the initial perturbation vorticity to be inside of the angular velocity maximum for the growth to occur. Enhanced eye-eyewall mixing by the prior wave-number 2 and 3 asymmetries may have provided that initial perturbation vorticity, but due to the lack of
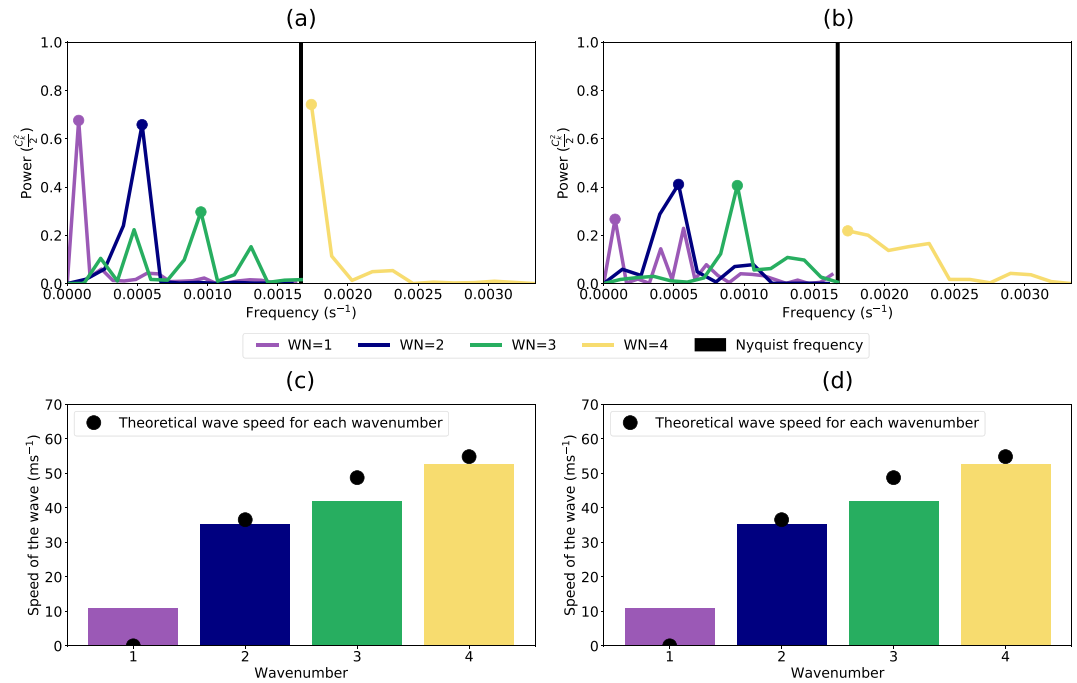
Figure 3. (a) Time-azimuth diagram of the wavenumber 2 tangential wind at $z = 3$ km averaged from $r = \text{RMW} - 3$ km to $r = \text{RMW} + 3$ km from 1020 to 1245 UTC 10 October. (b) The radial profile of axisymmetric absolute vertical vorticity derived from the P-3 dual-Doppler analysis (green) synthesized from 1100 to 1130 UTC, and the single-Doppler GVTD retrieval (blue) at $z = 3$ km on 1115 UTC 10 October, corresponding to the black line in (a). Radius-height diagram of azimuthal mean storm-relative (c) absolute vertical vorticity (shading), secondary circulation (vector), tangential wind (cyan contour), and RMW (white contour), (d) radial gradient of absolute vertical vorticity (shading), angular momentum surfaces (black contour), and RMW (white contour) from the P-3 dual-Doppler analysis.

scatterers in the eye, we cannot verify whether that was the case. Nolan and Montgomery (2000) showed that the presence of a wavenumber 1 algebraic instability causes the TC center to have trochoidal motion with respect to the time-averaged motion vector. The dynamic centers derived from aircraft in situ winds (Figure 1a) show a trochoidal motion from 1223 to 1430 UTC that is consistent with the theoretical growth of this instability.

Between 1330 and 1500 UTC, high wavenumbers 3 and 4 grew in amplitude as the wavenumber 1 amplitude decreased. The RMW contracted during this period and the mean vorticity in the inner core strengthened to greater than 6×10^{-3} s^{-1}. At 1530 UTC, the eyewall reflectivity pattern was triangular (Figure 1c), consistent with the retrieved wavenumber 3 wind asymmetry at this time. Subsequently, Michael gradually axisymmetrized as the mean vortex intensified and the asymmetric components of tangential wind weakened by 1630 UTC. The RMW then began to expand, and the magnitude of asymmetries increased again as the hurricane continued the northeastward trajectory and started to be impacted by the land interaction. Michael made landfall at 1730 UTC as the environmental VWS concurrently intensified and the hurricane intensity weakened significantly.

The analysis of Michael's inner core evolution suggests that the asymmetric VRW dynamics played an important role in modulating the structure and intensity changes. As described in section 1, previous observational analyses have yet to document the high-wavenumber kinematic structure propagation due to lack

Figure 4. Spectral time decomposition of $m = 1$–4: (a) tangential wind components and (b) reflectivity components. The Nyquist frequency is derived from the measuring frequency of the radar ($\sim 0.00167\,\mathrm{s}^{-1}$). The derived propagation speeds of each (c) tangential wavenumber and (d) reflectivity wavenumber and the theoretical VRWs propagation speed from the linear wave theory (black dot).

of both high spatial and temporal resolution data. Here, we use the GVTD retrieved asymmetric tangential winds as a proxy for vorticity and utilize the high temporal resolution to estimate the azimuthal propagation speed. Figure 3a shows an azimuth-time diagram of wavenumber 2 wind near the RMW during the period with a rotating elliptical eyewall. There is a clear cyclonic propagation of the wavenumber 2 amplitude during this time. Concurrent with this propagation, the mean vorticity structure derived from both P-3 dual-Doppler and single-Doppler radar analysis (Figure 3b) shows a steep vorticity gradient at the inner edge of the eyewall that would support VRW propagation. There is a good agreement in the retrieved axisymmetric vorticity across all radii, providing confidence in the radar analysis for investigating the vortex dynamics.

The enhanced sensitivity and pseudo dual-Doppler scanning strategy of the P-3 allow for a retrieval of the full axisymmetric kinematic structure at the time of the aircraft penetration (from 1100 to 1130 UTC 10 October). Figure 3c shows the radius-height azimuthal mean structure of vorticity, tangential wind, and secondary circulation. A local maximum of vorticity exceeding $9 \times 10^{-3}\,\mathrm{s}^{-1}$ is evident in the low levels, with a tower of positive vorticity extending to the upper troposphere. An updraft maximum in the upper levels suggests an ongoing development of the vorticity tower in the vertical. Due to the enhanced sensitivity of the P-3 radar in the storm, a reversal in the vorticity gradient at the inner edge of the eyewall is captured by the dual-Doppler analysis at upper levels and can be inferred at low levels (Figure 3d). The couplet of positive and negative radial gradient of vorticity satisfies the Rayleigh condition for barotropic instability that could support the exponential growth of higher order asymmetries. The tightly packed angular momentum surfaces in Figure 3d are nearly upright in low levels and slant outward in approximate congruence with the secondary circulation at upper levels.

The elliptical and triangle eyewall patterns are hypothesized to be the result of combined barotropic/baroclinic instability. The presence of the hollow vorticity tower during that period (Figure 3) suggests that wavenumber 2 and 3 modes could grow via barotropic/baroclinic instability (Terwey & Montgomery, 2002) and result in vorticity mixing between the eye and eyewall. This vorticity mixing can transport the perturbation vorticity into the core and can lead to weakening of the symmetric vortex. In Hurricane Michael,

however, sustained deep convection and vortex stretching were evidently able to maintain and intensify the symmetric vorticity tower despite the growth of asymmetric perturbations.

Power spectrum analyses in the frequency domain of the tangential wind and reflectivity were performed in order to calculate the propagation speed of the asymmetries quantitatively (Figures 4a and 4b). In the supporting information S1, we provide the details of the power spectrum analysis. The asymmetric tangential winds have clearly separated spectral peaks that correspond to different azimuthal propagation speeds. The asymmetric reflectivity spectra have distinguishable peaks for the propagation signals for low wavenumbers ($m = 1$ and 2), whereas the high wavenumber signals ($m > 2$) are noisier and have multiple peaks of signal making it harder to recognize the propagation velocity.

Figures 4c and 4d display the theoretical speed calculated from Equation S1 and the observed speed. The strongest power of each wavenumber is selected as the observed VRW propagation velocity. In the supporting information S1, we provide the derivation of azimuthal velocity of each wavenumber. The observed values are remarkably consistent with the linear wave theory, suggesting that the observed asymmetries are well described by VRW theory. Moreover, the propagation speeds of asymmetric reflectivity signals are also consistent with the linear wave theory (Figure 4d) despite the broader power spectra. The observed asymmetric propagation of both wind and reflectivity provides further support for the theoretical framework of linear wave theory, suggesting that nonlinear wave interaction may be of secondary importance in the propagation speed.

The similar propagation speed of tangential wind and reflectivity at the altitude of 3 km implies that the vorticity and divergence fields are coupled together in the low to mid-troposphere. Due to sampling limitations of the radar beam, it is unclear whether this coupling originates in the boundary layer or is only in the free troposphere. Kuo et al. (2016) used a nondivergent barotropic model for the free atmosphere and an asymmetric slab boundary layer underneath and found a tangential wind maximum at the minor axis of the elliptic vortex in the free atmosphere, whereas the wind maximum was closer to the major axis within the boundary layer. In a real, baroclinic vortex that decays with height, the theoretical wave speed for VRWs is height dependent such that a vertically coherent asymmetry that propagates at the same speed over some depth will deviate from the theory at different levels. While Michael's symmetric vorticity tower was quite strong through the depth of the troposphere (Figure 3c), the mean flow still decayed with height suggesting barotropic theory cannot fully describe the evolution. The good correspondence between theoretical and observed wave speeds does indicate that barotropic theory is a reasonable approximation in this case.

Previous studies have shown that the vortex structure and the location of diabatic heating play important roles in the intensification of TCs (Schubert & Hack, 1982). Latent heat release is the leading order effect in PV generation in the TC inner core and VRWs can transport the diabatically generated PV inward (Chen & Yau, 2001). In barotropic models, mixing associated with VRW activity leads to weakening of the symmetric vortex. The simultaneous amplification of symmetric vortex (Figure 2b) and cycles of intensification and weakening of asymmetries (Figure 3d) throughout the RI stage suggest that the asymmetries are not necessarily a negative impact on TC intensification, consistent with the recent study by J.-D. Lee and Wu (2018). Whether the vortex would have intensified even more rapidly in the absence of the asymmetries is unknown and remains to be explored with numerical modeling in future work.

4. Conclusion

The structure and evolution of Hurricane Michael were examined using single-Doppler radar observations, providing the first observational evidence of the evolving wind field of a polygonal eyewall during RI to Category 5 intensity. Quantitative evidence of growing structures with low (1–4) azimuthal wavenumbers in the tangential wind and reflectivity fields suggests the presence of rapidly evolving VRWs. A spectral time decomposition analysis of the retrieved winds indicates that the propagation speeds of different VRWs are consistent with linear wave theory on a symmetric radial vorticity gradient. The appearance and growth of the asymmetries are proposed to be the result of a combination of wavenumber 1 algebraic instabilities and higher order barotropic/baroclinic instabilities. Aircraft center fixes document a period of trochoidal motion with an enhanced wavenumber 1 asymmetry when all other higher wavenumber asymmetries were suppressed. A period of higher order VRW growth followed as the mean radial vorticity gradient amplified and the hollow vortex tower contracted, eventually becoming nearly symmetric prior to landfall. The

simultaneous amplification of the symmetric vortex and cycles of growth and decay of asymmetries suggest that they were closely coupled. After Michael made landfall, both wind intensity and minimum pressure weakened significantly, and the asymmetries increased due to land friction and increasing vertical wind shear.

The results presented here highlight the value of coastal radar observations to investigate physical mechanisms of TC intensity and structure evolution with high temporal and spatial resolution. Airborne dual-Doppler radar analysis supports the single-Doppler wind retrievals and documents the vertical structure of the growing vorticity tower, indicating the necessary condition for barotropic/baroclinic instability. The evolution of the vorticity gradient derived from the single-Doppler analysis further presents new insights on intensity and structure change, which will help to improve TC forecasts in the future. In addition, both the reflectivity and tangential winds show evidence of polygonal structure and propagate at a similar speed, indicating that the vorticity and divergence fields are closely coupled together. The interaction between the asymmetric vortex dynamics and diabatic generation of PV by the convection may play a salient role in RI and is an important topic for future research.

Data Availability Statement

The data used in this paper are available through zenodo: https://doi.org/10.5281/zenodo.3928704.

References

Bell, M. M. (2019). nsf-lrose/lrose-blaze: lrose-blaze-20190105. https://doi.org/10.5281/zenodo.2532758

Bell, M. M., & Lee, W.-C. (2012). Objective tropical cyclone center tracking using single-Doppler radar. *Journal of Applied Meteorology and Climatology*, *51*(5), 878–896. https://doi.org/10.1175/JAMC-D-11-0167.1

Bell, M. M., Lee, W.-C., Wolff, C. A., & Cai, H. (2013). A Solo-based automated quality control algorithm for airborne tail Doppler radar data. *Journal of Applied Meteorology and Climatology*, *52*(11), 2509–2528. https://doi.org/10.1175/JAMC-D-12-0283.1

Bell, M. M., & Montgomery, M. T. (2008). Observed structure, evolution, and potential intensity of Category 5 Hurricane Isabel (2003) from 12 to 14 September. *Monthly Weather Review*, *136*(6), 2023–2046. https://doi.org/10.1175/2007MWR1858.1

Bell, M. M., Montgomery, M. T., & Emanuel, K. A. (2012). Air–sea enthalpy and momentum exchange at major hurricane wind speeds observed during CBLAST. *Journal of the Atmospheric Sciences*, *69*(11), 3197–3222. https://doi.org/10.1175/JAS-D-11-0276.1

Beven, J. L., Berg, R., & Hagen, A. (2019). Hurricane Michael (2018). National Hurricane Center Tropical Cyclone Report, 86.

Cha, T.-Y. (2018). Eyewall replacement cycle of Hurricane Matthew (2016) observed by Doppler radars (M. S. Thesis), Colorado State University.

Cha, T.-Y., & Bell, M. M. (2020). Comparison of Single Doppler and Multiple Doppler Wind Retrievals in Hurricane Matthew (2016). *Atmospheric Measurement Techniques Discussions*, *2020*, 1–23. https://doi.org/10.5194/amt-2020-240

Chen, Y., & Yau, M. K. (2001). Spiral bands in a simulated hurricane. Part I: Vortex Rossby wave verification. *Journal of the Atmospheric Sciences*, *58*(15), 2128–2145. https://doi.org/10.1175/1520-0469(2001)058<2128:SBIASH>2.0.CO;2

Corbosiero, K. L., Molinari, J., Aiyyer, A. R., & Black, M. L. (2006). The structure and evolution of Hurricane Elena (1985). Part II: Convective asymmetries and evidence for vortex Rossby waves. *Monthly Weather Review*, *134*(11), 3073–3091. https://doi.org/10.1175/MWR3250.1

DeMaria, M., Mainelli, M., Shay, L. K., Knaff, J. A., & Kaplan, J. (2005). Further improvements to the statistical hurricane intensity prediction scheme (SHIPS). *Weather and Forecasting*, *20*(4), 531–543. https://doi.org/10.1175/WAF862.1

Hendricks, E. A., McNoldy, B. D., & Schubert, W. H. (2012). Observed inner-core structural variability in Hurricane Dolly (2008). *Monthly Weather Review*, *140*(12), 4066–4077. https://doi.org/10.1175/MWR-D-12-00018.1

Hendricks, E. A., Peng, M. S., Fu, B., & Li, T. (2010). Quantifying environmental control on tropical cyclone intensity change. *Monthly Weather Review*, *138*(8), 3243–3271. https://doi.org/10.1175/2010MWR3185.1

Hendricks, E. A., Schubert, W. H., Chen, Y.-H., Kuo, H.-C., & Peng, M. S. (2014). Hurricane eyewall evolution in a forced shallow-water model. *Journal of the Atmospheric Sciences*, *71*(5), 1623–1643. https://doi.org/10.1175/JAS-D-13-0303.1

Itano, T., & Hosoya, M. (2013). Spectral analyses of the polygonal eye of Typhoon Sinlaku. *Monthly Weather Review*, *141*(3), 987–996. https://doi.org/10.1175/MWR-D-12-00122.1

Jou, B. J.-D., Lee, W.-C., Liu, S.-P., & Kao, Y.-C. (2008). Generalized VTD retrieval of atmospheric vortex kinematic structure. Part I: Formulation and error analysis. *Monthly Weather Review*, *136*(3), 995–1012. https://doi.org/10.1175/2007MWR2116.1

Kaplan, J., & DeMaria, M. (2003). Large-scale characteristics of rapidly intensifying tropical cyclones in the north Atlantic basin. *Weather and Forecasting*, *18*(6), 1093–1108. https://doi.org/10.1175/1520-0434(2003)018<1093:LCORIT>2.0.CO;2

Kossin, J. P., & Eastin, M. D. (2001). Two distinct regimes in the kinematic and thermodynamic structure of the hurricane eye and eyewall. *Journal of the Atmospheric Sciences*, *58*(9), 1079–1090. https://doi.org/10.1175/1520-0469(2001)058<1079:TDRITK>2.0.CO;2

Kuo, H.-C., Cheng, W.-Y., Yang, Y.-T., Hendricks, E. A., & Peng, M. S. (2016). Deep convection in elliptical and polygonal eyewalls of tropical cyclones. *Journal of Geophysical Research*, *121*, 14,456–14,468. https://doi.org/10.1002/2016JD025317

Kuo, H.-C., Williams, R. T., & Chen, J.-H. (1999). A possible mechanism for the eye rotation of Typhoon Herb. *Journal of the Atmospheric Sciences*, *56*(11), 1659–1673. https://doi.org/10.1175/1520-0469(1999)056<1659:APMFTE>2.0.CO;2

Lee, W.-C., & Bell, M. M. (2007). Rapid intensification, eyewall contraction, and breakdown of Hurricane Charley (2004) near landfall. *Geophysical Research Letters*, *34*, L02802. https://doi.org/10.1029/2006GL027889

Lee, W.-C., Jou, B. J.-D., Chang, P.-L., & Deng, S.-M. (1999). Tropical cyclone kinematic structure retrieved from single-Doppler radar observations. Part I: Interpretation of Doppler velocity patterns and the GBVTD technique. *Monthly Weather Review*, *127*(10), 2419–2439. https://doi.org/10.1175/1520-0493(1999)127<2419:TCKSRF>2.0.CO;2

Lee, W.-C., & Marks, F. D. (2000). Tropical cyclone kinematic structure retrieved from single-Doppler radar observations. Part II: The GBVTD-simplex center finding algorithm. *Monthly Weather Review*, *128*(6), 1925–1936. https://doi.org/10.1175/1520-0493(2000)128<1925:TCKSRF>2.0.CO;2

Lee, J.-D., & Wu, C.-C. (2018). The role of polygonal eyewalls in rapid intensification of typhoon Megi (2010). *Journal of the Atmospheric Sciences*, *75*(12), 4175–4199. https://doi.org/10.1175/JAS-D-18-0100.1

Martinez, J., Bell, M. M., Rogers, R. F., & Doyle, J. D. (2019). Axisymmetric potential vorticity evolution of Hurricane Patricia (2015). *Journal of the Atmospheric Sciences*, *76*(7), 2043–2063. https://doi.org/10.1175/JAS-D-18-0373.1

Martinez, J., Bell, M. M., Vigh, J. L., & Rogers, R. F. (2017). Examining tropical cyclone structure and intensification with the FLIGHT+ dataset from 1999 to 2012. *Monthly Weather Review*, *145*(11), 4401–4421. https://doi.org/10.1175/MWR-D-17-0011.1

Menelaou, K., & Yau, M. K. (2014). On the role of asymmetric convective bursts to the problem of hurricane intensification: Radiation of vortex Rossby waves and wave-mean flow interactions. *Journal of the Atmospheric Sciences*, *71*(6), 2057–2077. https://doi.org/10.1175/JAS-D-13-0343.1

Montgomery, M. T., & Shapiro, L. J. (1995). Generalized Charney–Stern and Fjortoft theorems for rapidly rotating vortices. *Journal of the Atmospheric Sciences*, *52*(10), 1829–1833. https://doi.org/10.1175/1520-0469(1995)052<1829:GCAFTF>2.0.CO;2

Moon, Y., & Nolan, D. S. (2015). Spiral rainbands in a numerical simulation of Hurricane Bill (2009). Part II: Propagation of inner rain-bands. *Journal of the Atmospheric Sciences*, *72*(1), 191–215. https://doi.org/10.1175/JAS-D-14-0056.1

Muramatsu, T. (1986). The structure of polygonal eye of a typhoon. *Journal of the Meteorological Society of Japan. Ser. II*, *64*(6), 913–921. https://doi.org/10.2151/jmsj1965.64.6913

Nolan, D. S., & Montgomery, M. T. (2000). The algebraic growth of wavenumber one disturbances in hurricane-like vortices. *Journal of the Atmospheric Sciences*, *57*(21), 3514–3538. https://doi.org/10.1175/1520-0469(2000)057<3514:TAGOWO>2.0.CO;2

Reasor, P. D., Montgomery, M. T., Marks, F. D., & Gamache, J. F. (2000). Low-wavenumber structure and evolution of the hurricane inner core observed by airborne dual-Doppler radar. *Monthly Weather Review*, *128*(6), 1653–1680. https://doi.org/10.1175/1520-0493(2000)128<1653:LWSAEO>2.0.CO;2

Rozoff, C. M., Kossin, J. P., Schubert, W. H., & Mulero, P. J. (2009). Internal control of hurricane intensity variability: The dual nature of potential vorticity mixing. *Journal of the Atmospheric Sciences*, *66*(1), 133–147. https://doi.org/10.1175/2008JAS2717.1

Schubert, W. H., & Hack, J. J. (1982). Inertial stability and tropical cyclone development. *Journal of the Atmospheric Sciences*, *39*(8), 1687–1697. https://doi.org/10.1175/1520-0469(1982)039<1687:ISATCD>2.0.CO;2

Schubert, W. H., Montgomery, M. T., Taft, R. K., Guinn, T. A., Fulton, S. R., Kossin, J. P., & Edwards, J. P. (1999). Polygonal eyewalls, asymmetric eye contraction, and potential vorticity mixing in hurricanes. *Journal of the Atmospheric Sciences*, *56*(9), 1197–1223. https://doi.org/10.1175/1520-0469(1999)056<1197:PEAECA>2.0.CO;2

Shimada, U., Sawada, M., & Yamada, H. (2018). Doppler radar analysis of the rapid intensification of Typhoon Goni (2015) after eyewall replacement. *Journal of the Atmospheric Sciences*, *75*(1), 143–162. https://doi.org/10.1175/JAS-D-17-0042.1

Smith, R. A., & Rosenbluth, M. N. (1990). Algebraic instability of hollow electron columns and cylindrical vortices. *Physical Review Letters*, *64*, 649–652. https://doi.org/10.1103/PhysRevLett.64.649

Terwey, W. D., & Montgomery, M. T. (2002). Wavenumber-2 and wavenumber-m vortex Rossby wave instabilities in a generalized three-region model. *Journal of the Atmospheric Sciences*, *59*(16), 2421–2427. https://doi.org/10.1175/1520-0469(2002)059<2421:WAWMVR>2.0.CO;2

Willoughby, H. E., & Chelmow, M. B. (1982). Objective determination of hurricane tracks from aircraft observations. *Monthly Weather Review*, *110*(9), 1298–1305. https://doi.org/10.1175/1520-0493(1982)110<1298:ODOHTF>2.0.CO;2

Wu, C.-C., Wu, S.-N., Wei, H.-H., & Abarca, S. F. (2016). The role of convective heating in tropical cyclone eyewall ring evolution. *Journal of the Atmospheric Sciences*, *73*(1), 319–330. https://doi.org/10.1175/JAS-D-15-0085.1